ELSEVIER

Solid State Ionics 131 (2000) 143–157

SOLID STATE IONICS

www.elsevier.com/locate/ssi

Ionic conduction in nanocrystalline materials

Harry L. Tuller*

Crystal Physics & Electroceramics Laboratory, Department of Materials Science & Engineering, Massachusetts Institute of Technology, 77 Massachusetts Ave, Room 13-3126, Cambridge, MA 02139, USA

Received 20 December 1999; received in revised form 2 February 2000; accepted 10 February 2000

Abstract

The potential impact of high densities of interfaces in nanocrystalline solids on ionic conduction and defect formation are examined. The literature on three oxides; cubic zirconia, ceria and titania, is reviewed. While it remains too early to make firm conclusions, the following observations are made. Additives which contribute to ion blocking at grain boundaries are diluted in nanocrystalline oxides giving rise to substantial reductions in specific grain boundary resistivities. The case for enhanced ionic conduction in nanocrystalline oxides remains unresolved due to conflicting reports and inadequate efforts to isolate the ionic from the total conductivity. There is strong support for the notion that the energetics for defect formation may be substantially reduced in nanocrystalline oxides leading to markedly increased levels of nonstoichiometry and electronic carrier generation.

Keywords: Ionic conductivity; Nanocrystalline; Zirconia; Ceria; Titania; Defects

1. Introduction

The influence of grain boundaries on the electrical, diffusive and defect properties of electroceramics has been recognized for some time. In ZnO varistors, for example, grain boundaries, depleted of free electrons, serve to increase the overall resistance of the device, at low fields, by a factor of $\approx 10^{10}$ [1]. Similarly, impurities such as SiO_2, known to segregate to the grain boundaries in stabilized zirconia and ceria, reduce the effective oxygen ion conductivity by as much as several orders of magnitude [2–5]. Alternatively, grain boundaries may serve as 'short circuiting pathways' as they do in $LiI–Al_2O_3$ composites leading to enhancements in Li ion conductivity by nearly two orders of magnitude [6]. Given the recent and rapidly growing interest in nanocrystalline solids, one logically questions the impact that this change in scale may have on the properties of solid state ionic materials. In this article, we consider why transport across or along grain boundaries in solids with nanometer-sized grains may differ distinctly from that in conventional polycrystalline solids. We also consider how defect generation may be influenced by the change in scale and the impact this may have on mixed ionic-electronic conduction (MIEC) in solids.

2. Impact of interfaces on ionic conduction

Since ions move by a thermally activated 'hopping' motion between near equivalent sites, high

*Tel.: +1-617-253-6890; fax: +1-617-258-5749.
E-mail address: hltuller@mit.edu (H.L. Tuller)

0167-2738/00/$ – see front matter
PII: S0167-2738(00)00629-9

temperature operation is normally required to achieve reasonably high levels of ionic conductivity in most ionic solids. Well-known exceptions exist such as αAgI and some Ag and Li-based oxide and sulfide glasses [7] which exhibit high levels of ionic conductivity at or in the near vicinity of room temperature. This follows from the fact that they are simultaneously highly disordered and exhibit continuous, open channels between ion sites.

In contrast to the above two examples, in which the source of ionic disorder is intrinsic in nature, stabilized cubic zirconia (e.g. $Zr_{1-x}Y_xO_{2-x/2}$) is a well-known example in which disorder is induced by the addition of aliovalent elements. Nevertheless, temperatures of the order of 900–1000°C are required to reach levels of ionic conductivity of ≈0.1 S/cm, given the much larger ionic radius of oxygen and consequently lower mobility.

A number of oxygen ion conductors, largely stabilized zirconia, ceria and lanthanum gallate are prime candidates to serve as the solid electrolyte in the solid oxide fuel cell. For reasons related to long-term stability and cost, one would like to drop the operating temperature of these devices by at least several hundred degrees. Decreased temperatures, however, require increased electrolyte conductance and enhanced gas/electrode reaction kinetics. An intriguing question is whether polycrystalline ceramics, with nanosize grains, would exhibit enhanced ionic conduction due to transport along the grain boundaries.

It is indeed well-known in the materials community that grain boundary diffusion is often orders of magnitude greater than corresponding 'bulk' diffusion through the grains. This is illustrated in the classic diffusion studies on NiO [8] as illustrated in Fig. 1 in which, for example, the oxygen grain boundary diffusivity at ≈1300°C is reported to be approximately six orders of magnitude higher than that in the lattice. Presumably, the source of enhanced diffusion results from the fact that a high percentage of displaced atoms with corresponding strained bonds and excess volume exist at the interface between the misaligned adjacent grains. Grain boundaries thus intrinsically appear to possess the two key characteristics necessary for enhanced ionic diffusion: high defect densities (displaced atoms) and high mobilities (interconnected excess

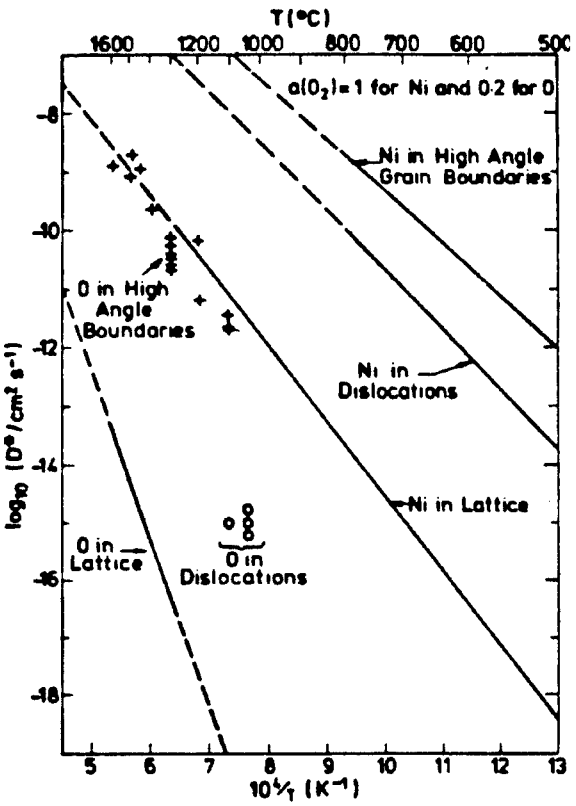

Fig. 1. Nickel and oxygen self-diffusion in bulk, in dislocation and in grain boundaries of nickel oxide [8].

free volume). There are, however, surprisingly few cases in which the source of the enhanced diffusion at grain boundaries has been well established.

High ionic diffusivities are insufficient by themselves to insure high ionic conductivities. Indeed, in conventional polycrystalline materials, the fractional cross-sectional area of grain boundaries lying parallel to the current flux is very small. Consider the idealized 'brick model' schematic in Fig. 2, in which cubic grains with dimension L on each side are separated from each other by grain boundaries of width $2b$. Ignoring blocking effects of boundaries perpendicular to current flow, the relative ratio of cross-sectional areas is

$$\frac{A(\text{grains})}{A(\text{boundaries})} = \frac{L}{4b} \tag{1}$$

Thus to achieve equal conductance, the grain bound-

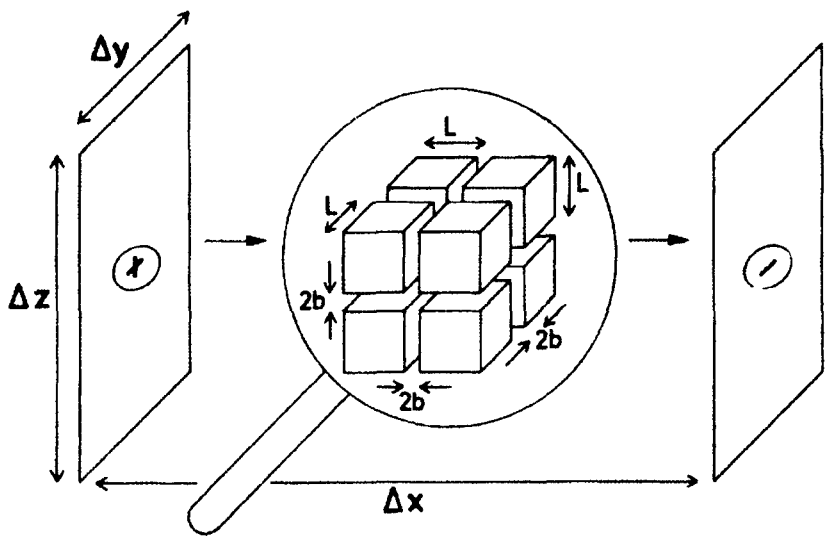

Fig. 2. Brick layer model of idealized polycrystalline structure in which grains of dimensions L^3 are separated by grain boundaries of width $2b$ [6].

ary conductivity σ_{gb} must be larger than the grain conductivity σ_B by

$$\sigma_{GB} = \sigma_B(L/4b) \tag{2}$$

For a typical polycrystalline material with average grain size of 1 μm and a grain boundary core width of 1 nm, $\sigma_{GB} \approx 500\sigma_B$ is required to merely double the overall conductance of the material.

Consider instead the schematic of a nanocrystalline solid in Fig. 3 in which the dimensions of the grain boundaries become comparable to those of the grains. Here a significant fraction of the atoms lie in the disordered region of the boundaries and can be expected to contribute to enhanced conductivity. Thus for geometries for which $L \approx 4b$, a grain boundary conductivity which is, say, several orders of magnitude greater than that in the bulk will translate into a similar enhancement (less a factor of 2) in the overall ionic conductivity of the specimen.

The intuitive image of a highly disordered grain boundary region, as depicted in Fig. 3, is not born out by high resolution transmission electron microscopy. It is instructive to examine the high resolution microscopy images of NiO obtained by Merkle [10] and reproduced in Fig. 4. One observes that structural disorder in the grain boundary 'core' is accomodated within several atomic planes of the boundary and rather than being randomly dispersed, 'defects' organize themselves and create a new periodic structure at the interface. Indeed, recent TEM observations of nanocrystalline ceria [11] show crystallites with high levels of perfection separated by atomically sharp boundaries with no indication of the glass-like disorder discussed in the early diffusion literature.

An additional explanation for enhanced conduction at boundaries is related to the formation of space charge regions in the grains adjacent to the boundaries. Charged species, impurities and/or defects, tend to segregate to the grain boundaries in order to lower the strain and electrostatic energies of the system. These boundary charges are compensated by the formation of space charge in the adjoining grains. Thus, bulk ionic defects with like charge to that of the boundary will be depleted while those with opposite charge will be accumulated in the space charge region. If the bulk defect with high mobility is accumulated in the space charge region, the overall conductivity of the solid should increase. The width of this space charge region is tied to the Debye screening length, L_D

$$L_D = (\epsilon_r \epsilon_0 k/Tq^2 C_b)^{1/2} \tag{3}$$

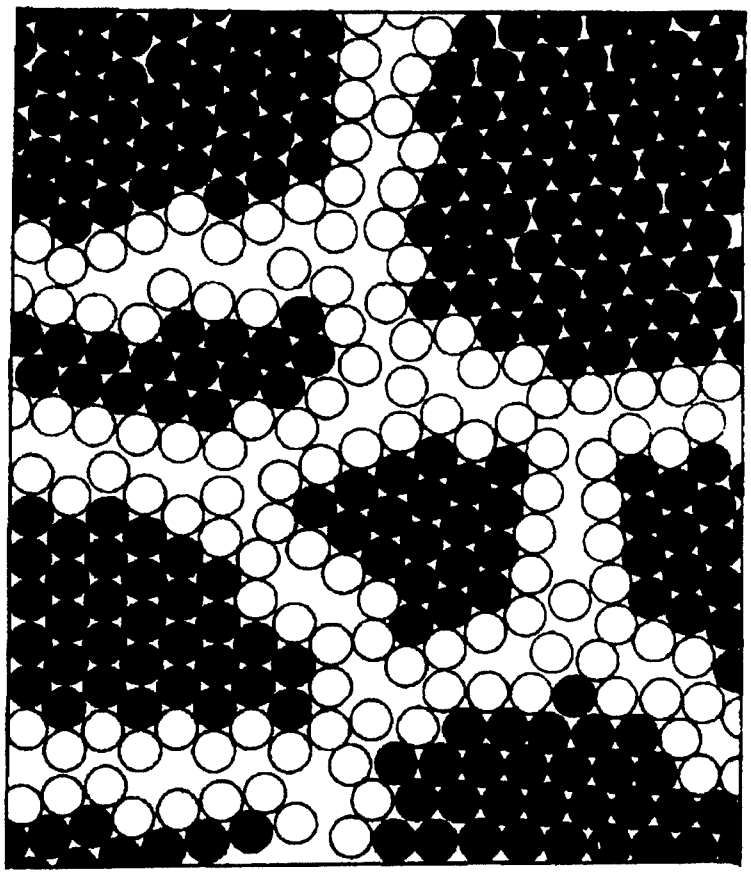

Fig. 3. Schematic of grains (dark circles) separated by grain boundary regions (open circles) of comparable dimensions [9].

in which C_b is the concentration of the bulk majority carrier. For a solid with $\epsilon_r = 10$ and $C_b = 10^{22}$ m^{-3} at 600 K, this leads to a Debye length of ≈ 50 nm and a space charge width of approximately two times that value. Thus, the effective boundary width contributing to enhanced conductivity may be many times greater than the boundary core width.

Maier [6] has calculated the additional boundary contribution, $\Delta\sigma_m$, to be

$$\Delta\sigma^m = (4L_D/d)(\sigma_{v,sc} + \sigma_{i,sc}) \quad (4)$$

in which d is the average grain size and $\sigma_{v,sc}$ and $\sigma_{i,sc}$ are the mean space charge conductivities due to vacancies and interstitials respectively. The boundary contribution is, thus, given by the product of the areal fraction of the interface and the mean space charge conductivity. Obviously, as L_D approaches d, as it does in nanocrystalline solids, this contribution can become significant. However, an additional factor must be taken into account under these circumstances.

As illustrated in Fig. 5, as d approaches L_D, the defect density at the center of the grain no longer reverts back to the background value C_b. Thus, in the limit of small grains, local charge neutrality is nowhere satisfied. Under these circumstances, Maier has shown that an additional nano-size factor g, given by [12]

$$g = (4L_D/d)[(C^\circ - C_b)/C^\circ]^{1/2} \quad (5)$$

where C° is the concentration of the majority mobile defect at the first layer adjacent to the interface core,

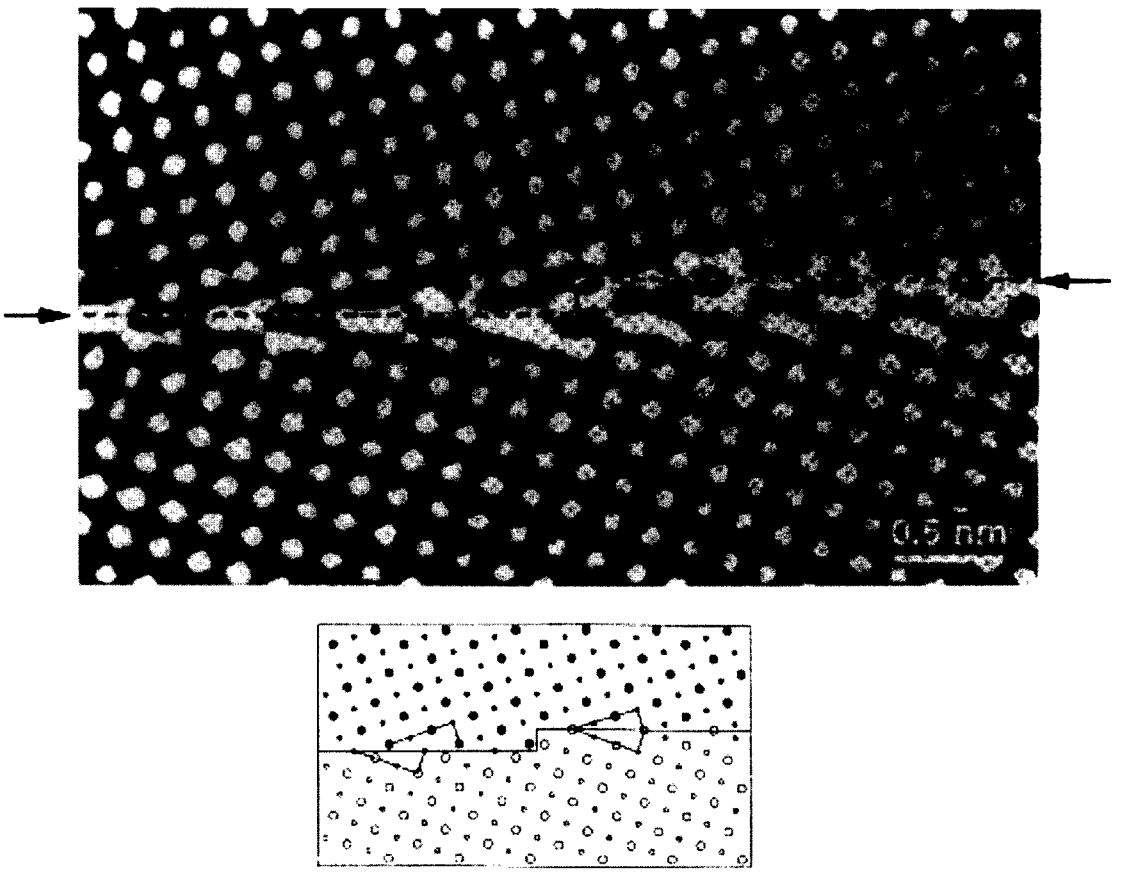

Fig. 4. High resolution electron micrograph, above, and a calculated image, below, of a (310) symmetric <100> tilt boundary in NiO [10].

further enhances the grain boundary contribution to the conductivity compared to the case where $d \gg L_D$. For large C° ($\gg C_b$), $g \approx (4L_D/d)$ which reaches an order of magnitude for $d = 0.4L_D$ [12].

In the last few years, a number of oxides known to exhibit ionic conductivity, such as stabilized zirconia and ceria, have been prepared in nanocrystalline form and their transport properties have been reported. In the following, we review these results, focusing particularly on the trend in magnitude of both ionic and electronic conductivity as the average grain size is reduced to the nanometer regime. Our interest in the electronic conductivity derives from the apparent change in defect thermodynamics at the nanometer scale. This translates into reduced defect formation energies and, under certain circumstances, markedly enhanced electronic conductivities which may mask increases in the ionic conductivity. This may be detrimental for applications in which one wishes to utilize the material as a solid electrolyte or beneficial where the requirement is for high levels of mixed ionic-electronic conductivity as in fuel cell electrodes or in oxygen permeation membranes [13].

Another feature which deserves particular attention is the influence of grain boundaries lying perpendicular to the flow of current. As mentioned at the beginning of this article, such boundaries often block the flow of current, and as the grain size decreases, could contribute to an overall decrease in conductivity. Thus, in analyzing the effects of grain size on conductivity, it is important to able to comment on the relative effects of boundaries both parallel and perpendicular to the flow of current. In the literature published to date, this information is

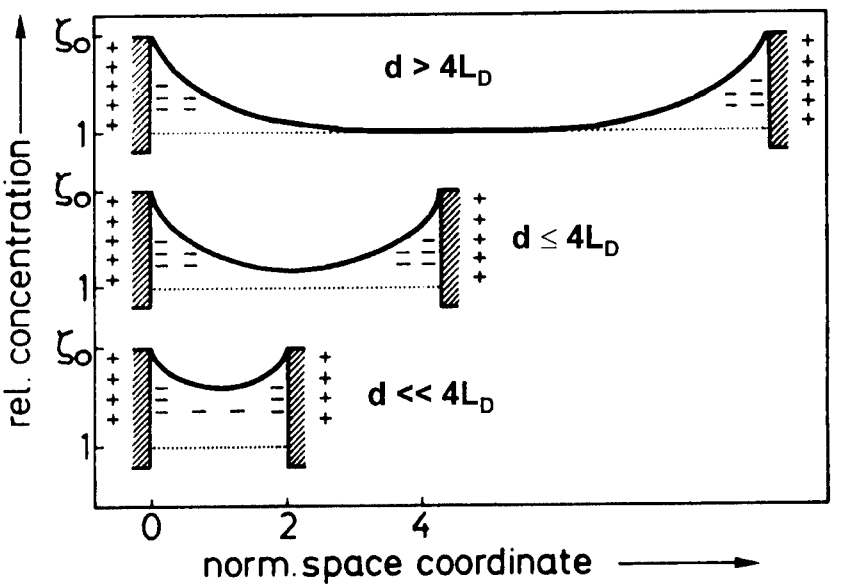

Fig. 5. Defect profiles in structures with dimension, d. The build defect concentration is not reached when $d \ll 4L_D$, where L_D is the debye length [12].

often difficult to assess. Finally, we consider recent evidence for ionic conductivity in nano-crystalline TiO_2, an oxide normally viewed as a semiconductor.

3. Ion transport in nanocrystalline oxides

3.1. Stabilized zirconia

A recent study by Aoki et al. [5] reports perhaps the clearest correlation between grain size and ionic conductivity. In this study of high purity 15 mol% CaO-stabilized zirconia, a clear correlation was established between the amount of Si segregated to grain boundaries, as established by high resolution STEM, and the corresponding grain boundary resistivity, as derived by complex impedance measurements. The solute coverage in this high purity material could be systematically varied by changing the grain size over a 0.1–10 μm range at constant impurity and doping levels.

Of particular interest to this work are the results shown in Fig. 6, which show that the specific grain boundary conductivity drops sharply initially with increasing grain size and ultimately saturates above ~4 μm. This drop in specific grain boundary conductivity by about a factor of 15 is correlated with a corresponding increase in silicate ($Si_2Ca_3O_7$) coverage of the grain boundaries. Note, first, that in the regime of these studies, the solute coverage averages below a monolayer, and second, that the strongest dependence of grain boundary resistance on silicate

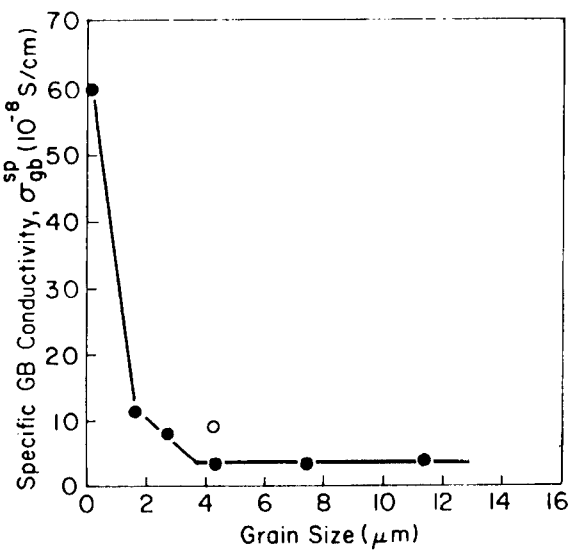

Fig. 6. Specific grain boundary conductivity in calcia stabilized zirconia at 500°C vs. grain size [5].

coverage occurs at low coverage levels. These results suggest that grain boundary resistance due to blocking effects at perpendicular boundaries may drop to exceptionally low values in relatively pure (relative to segregants such as Si) nanocrystalline conductors. This seems to be born out, at least, in some subsequent studies.

While the work by Aoki et al. [5] demonstrated a clear dependence of grain boundary conductance on grain size, the smallest grain size examined, 140 nm, was larger than that normally associated with nanocrystalline solids, i.e. typically several to 100 nm. In the following, we review studies performed on stabilized zirconia ceramics with grain sizes falling into this category.

Mondal and Hahn [14] prepared nanocrystalline zirconia stabilized with 2–3 mol% yttria beginning with powders processed by the inert-gas condensation technique and followed by sintering. The resultant specimens had grain sizes between 35 and 50 nm and relative densities between 82 and 93%. Activation energies for bulk (0.85±0.05 eV) and grain boundary conductivity (1.0±0.1 eV) as well as absolute values of conductivity coincided with that of conventional ceramics as illustrated in Fig. 7. The absence of significant effects was attributed to the insufficiently small grain sizes of their samples. Jiang et al. [15] reached similar conclusions. They prepared ultra-fine grained yttria-stabilized zirconia by combustion synthesis using metal nitrates as precursors. Compressed pellets were sintered by fast-firing at 1200–1400°C. Relative density was less than 95% for average grain sizes less than 200 nm. They also found activation energies for grain and grain boundary conduction (0.95 and 1.2 eV) to be in agreement with values for materials with micron-sized grains. Here, the grain size was even larger; over 90 nm in all cases.

On the contrary, Kosacki et al. [16], who investigated yttria (16%)-stabilized zirconia (YSZ) thin films prepared by a polymer precursor process on alumina substrates, found that the nanocrystalline materials exhibited a two order of magnitude increase in conductivity compared to polycrystalline and single crystalline materials. Fig. 8 compares the impedance spectra obtained for single, poly and nanocrystalline YSZ. A clear grain boundary (gb) contribution at intermediate frequencies is evident in the impedance spectra of polycrystalline YSZ with grain size above 1 μm. For nanocrystalline YSZ, a single semicircle, obtained at high frequency is attributed to the superposition of bulk and grain boundary effects. The bulk conductivities, as determined from the high frequency intercepts on the real axis for single and polycrystalline YSZ (grain size ≥1.3 μm) show no dependence on grain size as

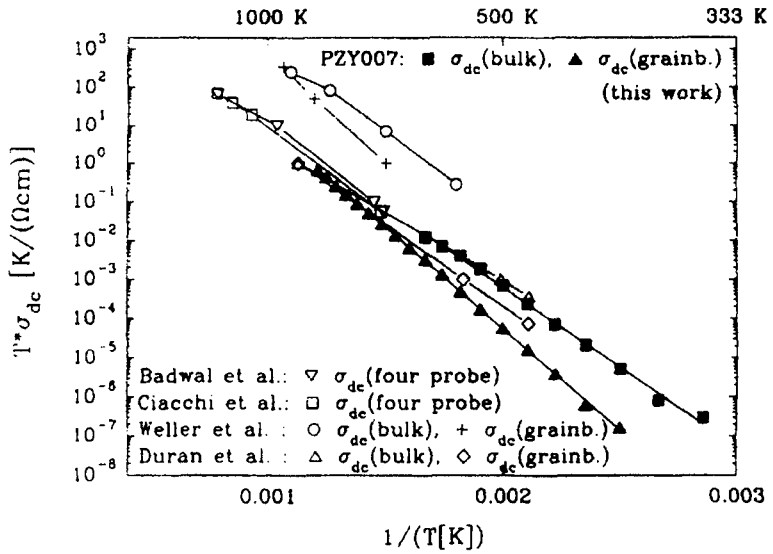

Fig. 7. Comparison of bulk and grain boundary conductivities of nano- and micro-crystalline YSZ [14].

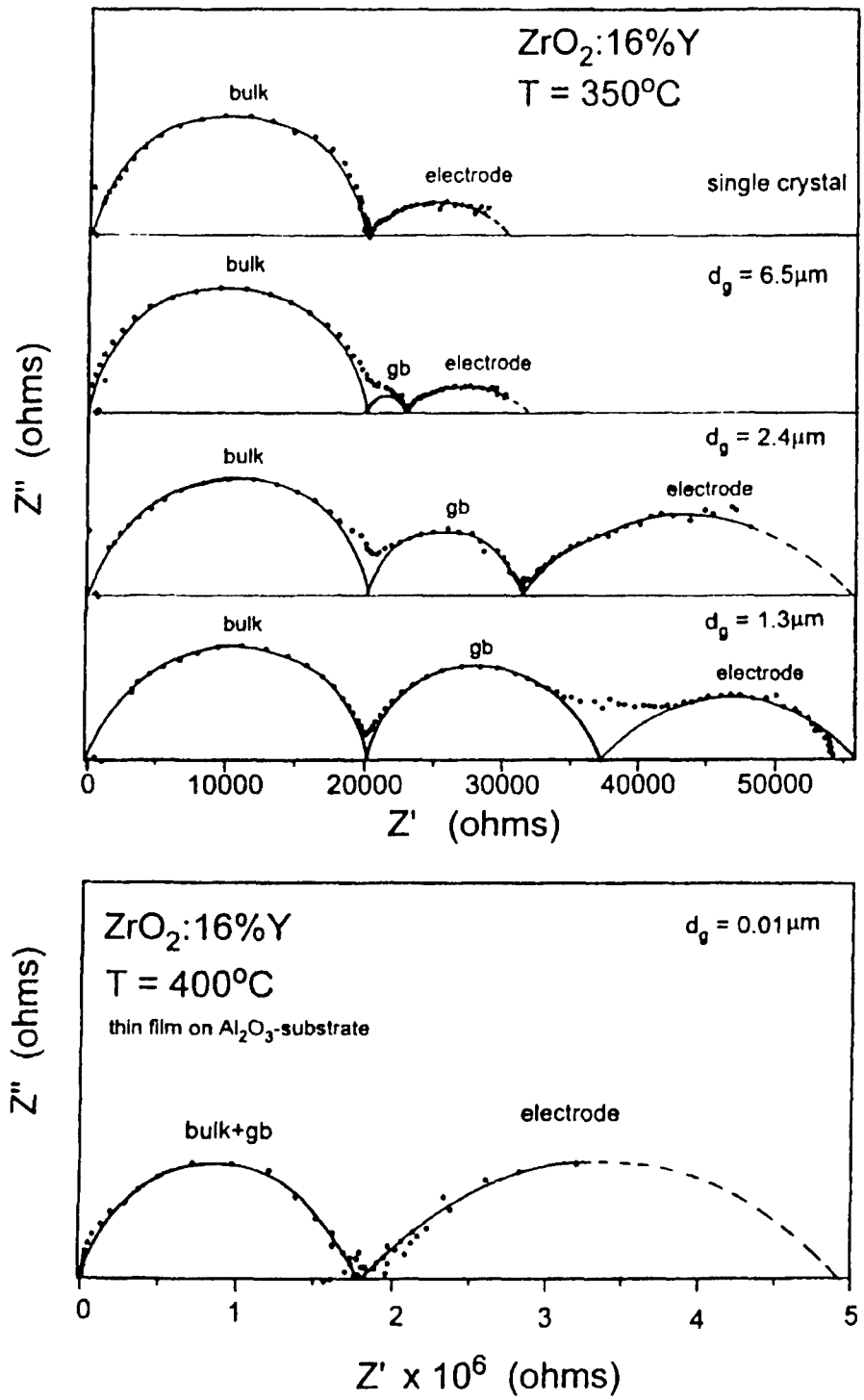

Fig. 8. Complex impedance spectra obtained for (a) single crystal microcrystalline YSZ bulk specimens and (b) for nanocrystalline YSZ films [16].

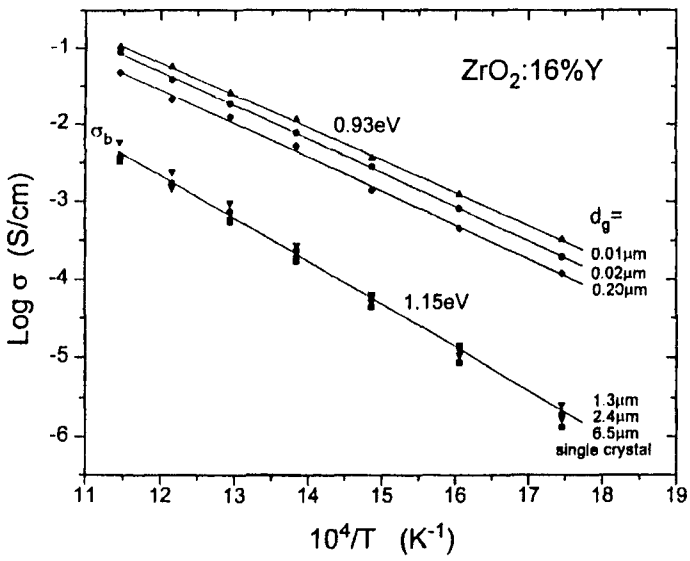

Fig. 9. Comparison of electrical conductivity for single crystal, bulk microcrystalline specimens and nanocrystalline thin films of YSZ [16].

evident from Fig. 9. On the other hand, the corresponding data for polycrystalline YSZ with submicron size grains show a substantial enhancement in conductivity above that of the larger grain materials. This increase in conductivity is associated with a reduction of the activation energy from 1.15 to 0.93 eV. The authors suggest that the high frequency resistance of the nanocrystalline YSZ is largely determined by the grain boundary resistance and attribute the sharp drop in the specific grain boundary resistance to a decrease in the level of impurities segregating to the boundaries as in Ref. [5]. It must be noted, however, if much of the high frequency resistance is attributed to grain boundary blocking, this would imply even higher bulk conductivity enhancements than those suggested in Fig. 9.

At this time, one can only speculate about the origin of the large discrepancy between the study of Kosacki et al. [16] and those of Mondal and Han [14] and Jiang et al. [15]. The key difference between these studies is the manner in which the nanocrystalline specimens were prepared. In Ref. [16], thin films of about 1 μm thickness were prepared by a polymer precursor spin coating process, while in Refs. [14,15], bulk specimens were prepared by pressing and sintering ultra-fine powders prepared by combustion synthesis or inert-gas condensation. Since films have a large surface to volume ratio, they tend to be more susceptible to the influence of humidity on the exposed side and film-substrate interactions on the opposite side. Control experiments in which alternate substrates are used and the relative humidity is varied under controlled conditions would help in clarifying the source of enhanced ionic conduction in thim film nanocrystalline YSZ.

3.2. Ceria

3.2.1. Undoped ceria

In contrast to stabilized zirconia, ceria (CeO_2) is stable in the cubic fluorite phase without the need for additives. Ce^{4+} reduces to Ce^{3+} at elevated temperatures and reducing atmospheres resulting in a high degree of oxygen deficiency and n-type semiconductivity [17,18]. Doping with acceptors such as Y^{3+} or Gd^{3+}, like YSZ, transforms ceria into an excellent solid oxide electrolyte [19]. These features appear to contribute to ceria's unusual catalytic activity. In particular, high surface area nanocrystalline CeO_{2-x} exhibits exceptionally high catalytic activity already at low temperatures in redox reactions such as CO oxidation and SO_2 reduction by CO [20].

It is of interest to establish the source of the enhanced catalytic activity of nanocrystalline ceria. To that end, Tschope et al. [21] examined the

electrical properties of porous nanocrystalline ceria as a function of temperature and at several different atmospheres. A typical complex impedance plot, which exhibits strong overlap between two semicircles, is shown in Fig. 10. Also shown is the fitted equivalent R–C circuit. The two capacitances were found to be within an order of magnitude of each other, not surprising given that the grain size in nanocrystalline solids approaches the same order of magnitude as the space charge width. This illustrates that the distinction between bulk and grain boundary regions tends to vanish as the grain size is reduced to the nanometer regime [21], consistent with observations for YSZ [16] as well as for other studies of CeO_2 [11] and TiO_2 [22].

The activation energy for conduction in porous nancrystalline CeO_2 (0.7 eV) was found to be less than half of that reported for single crystalline CeO_2 (1.97 eV) [8] pointing to a reduced enthalpy of defect formation. Because porous materials are more difficult to interpret due to uncertainties related to open porosity, surface adsorption and constrictions at particle contacts, Chiang et al. [11] prepared CeO_{2-x} polycrystals of ~10 nm grain size with densities of greater than 95% by several processing routes. These included powders prepared by inert gas condensation and by a chemical route. Both sets of powders were densified at 1.1 GPa pressure at 600°C for ~1 h thereby maintaining an average grain size of ~10 nm. Reference specimens of ~5 μm grain size were prepared by firing identical nanocrystalline pellets at 1200°C for 12–15 h. This allowed for one-to-one comparison between specimens which differed ideally only in microstructure.

The bulk conductivity (T=600°C), as derived from the high frequency part of the impedance spectra, is shown plotted in Fig. 11 as a function of P_{O_2} for the 10 nm and 5 μm grain size materials. Note that while the large grained material is P_{O_2}-independent at high P_{O_2} suggesting ionic conduction, nanosized material is P_{O_2} dependent, indicative of n-type semiconducting behavior. Furthermore, if one extrapolates the electronic conductivity of the 5 μm material to 10^5 Pa (1 atm), one observes ~10^4 enhancement in electronic conductivity for the nanocrysatlline material. As in the above study [21], the activation energy for electronic conduction is much reduced in nanocrystalline CeO_2 (0.99–1.16 eV) as compared to the coarsened material (2.45 eV). Kosacki et al. [23] found similar results for thin film CeO_2.

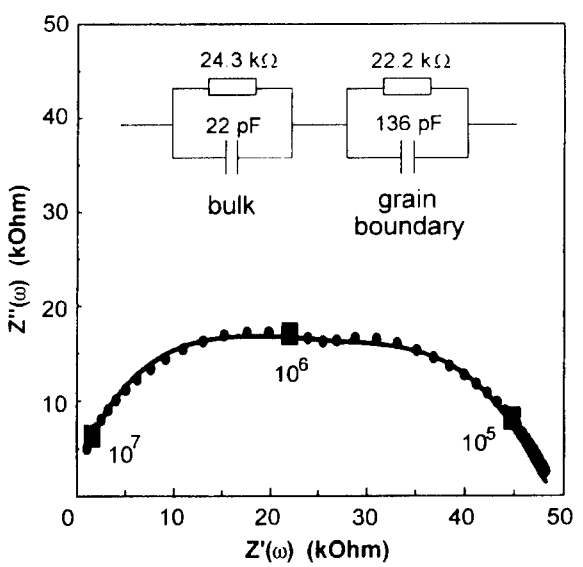

Fig. 10. Complex impedance spectrum of nanocrystalline CeO_{2-x} at 130°C in a hydrogen atmosphere and equivalent circuit [21]. Note strong overlap of high and low frequency semicircles.

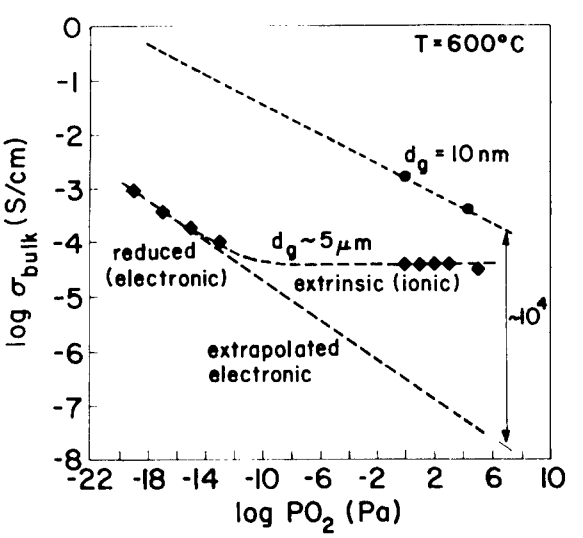

Fig. 11. The bulk conductivity of nanocrystalline (d~10 nm) and coarsened microcrystalline (d~5 mm) CeO_{2-x} measured at 600°C as a function of oxygen partial pressure [11].

One may relate these energies to the enthalpy of reduction by considering the appropriate reduction reaction

$$O_O \leftrightarrow V_O^{\cdot\cdot} + 2e' + \frac{1}{2}O_2(g) \quad (6)$$

which for dilute concentrations has the mass action relation

$$K_R(T) = K_R^\circ \exp\left(-\frac{\Delta H_R}{kT}\right) = [V_O^{\cdot\cdot}]n^2 P_{O_2}^{1/2} \quad (7)$$

Assuming the vacancy density is fixed by acceptor impurities as evident in Fig. 11 for the coarsened material and noting that the activation energy for conduction is given by

$$E_a = \left(\frac{\Delta H_R}{2}\right) + E_h \quad (8)$$

where E_h (=0.4 eV) is the hopping energy of electrons [18], one derives ΔH_R values of 1.18–1.52 eV for nanocrystalline CeO_2 versus 4.10 eV for coarsened CeO_2. This large dependence of the effective reduction enthalpy on grain size suggests, as in Ref. [20], that defect generation at grain boundaries and surfaces becomes predominant as these interfaces become more predominant.

Porat et al. [24] investigated the non-stoichiometry of nanocrystalline CeO_2 by coulometric titration. Large apparent deviations from stoichiometry of up to 10^{-3} were found. The oxygen deficiency follows an oxygen pressure dependence with an exponent of $-1/2$. This can be understood if neutral oxygen vacancies are majority defects in nanocrystalline CeO_2 or that oxygen losses upon reduction are largely due to oxygen desorption from particle surfaces. The latter interpretation corroborates the conclusions of Tschöpe and Birringer [25], who investigated chemically precipitated cerium dioxide annealed at 550 and 600°C by thermogravimetry. Pressure/composition isotherms at 500, 550 and 660°C of nanocrystalline and conventional polycrystals showed a two-phase region only at the highest temperature, where bulk reduction was observed. At lower temperature, surface oxygen was desorbed with the larger apparent oxygen deficiency of nanocrystalline materials correlated with the larger surface area.

3.2.2. CeO_2 solid solutions

Large deviations from stoichiometry were also found in nanocrystalline CeO_2–PrO_x solid solutions by Knauth and Tuller [26]. Of special note was the observation of chemical diffusivities with low activation energy of 0.3 eV. This is suspected to reflect the presence of fast diffusion pathways.

Chiang and coworkers [27,28] investigated highly dense gadolinium-doped cerium dioxide samples with about 10 nm average crystallite size. With a relatively small gadolinium concentration (1.5 mol%), qualitatively similar results with the nominally undoped samples were found: a strongly enhanced electronic conductivity and a small reduction enthalpy. This is experimental support for 'undoping' of grains due to the small grain size [5]. The grain boundary resistance was higher, likely because of gadolinium segregation. In heavily doped nanocrystalline CeO_2 samples (26 mol%), no significant increase in bulk ionic conductivity compared with a conventional sample was found. It appears that transport along grain boundaries, which is likely to be seen together with the bulk response, did not play a significant role, neither by ionic diffusion in interface cores nor in space charge regions due to carrier accumulation. In total, reduction of grain size resulted in an increase of total resistance and the grain boundaries remained highly blocking, even in nanocrystalline samples.

3.3. Titania

Nanocrystalline titanium dioxide is being exploited as the active element in inexpensive photovoltaic cells and as the photocatalyst in water treatment plants to oxidize dissolved organics [29,30]. It is also one of a number of semiconducting oxides which has been considered as a potential oxygen sensor. It is therefore of interest to establish if nanostructured titania exhibits enhanced ionic diffusion and/or defect generation.

Knauth and Tuller [22] prepared dense (~95%) compacts of TiO_2 with the anatase phase. The average grain size was 35 ± 10 nm. The P_{O_2} dependence of the electrical conductivity is shown plotted

in Fig. 12. In contrast to the p-to-n transition exhibited by coarsened titania at intermediate P_{O_2}, one observes an apparent ionic plateau at high P_{O_2} and an n-type regime at low P_{O_2}. The $P_{O_2}^{-1/2}$ dependence of the n-type conductivity is distinctly stronger than the $P_{O_2}^{-1/4}$ dependence exhibited by the coarsened material.

The ionic conductivity is shown plotted in Fig. 13 as a function of reciprocal temperature. The ionic conductivity is described by

$$\sigma_{ion} = \left(\frac{2.2 \times 10^3}{T}\right) \exp\left(-\frac{1\,eV}{kT}\right) \text{S/cm} \quad (9)$$

This corresponds to an ionic conductivity of ~2×10^{-5} S/cm at 1000 K. In a recent study on single crystalline titania, Nowotny et al. [31] were able to extract the ionic conductivity from the P_{O_2} dependence of the total conductivity. Interestingly enough, they obtained a similar value of $\sigma_{ion} \sim 3\times 10^{-5}$ S/cm at 1000 K but report a considerably larger activation energy of ~1.5 eV. This comparison suggests that while the effective doping level in the nanocrystalline material is lower due to segregation of dopants to the grain boundaries, the increased density of interfaces, at the same time, provides higher diffusive pathways than available in the single crystal material. This latter factor is presumably the source of the lower activation energy in the nanocrystalline material.

Demetry and Shi [32] found P_{O_2} independent conductivity plateaus at 500°C for rutile nanocrystal-

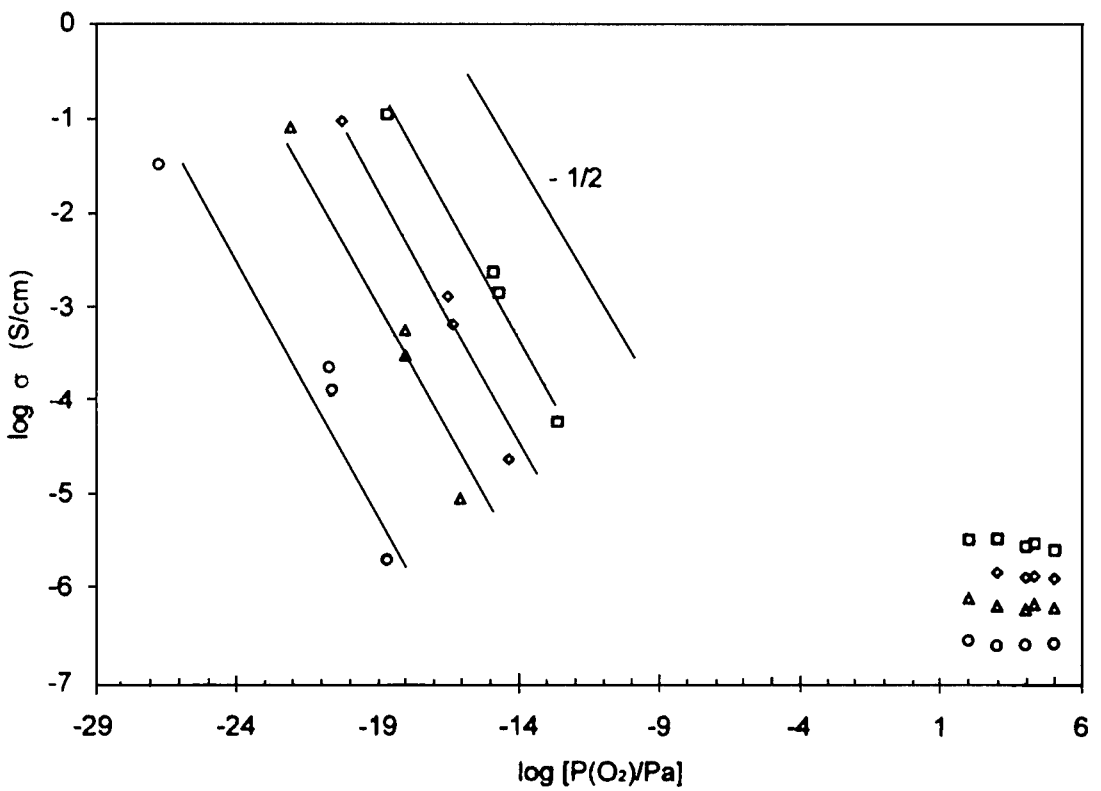

Fig. 12. Oxygen partial pressure dependence of the electrical conductivity of nanocrystalline TiO_2 (d~35 nm): □, 580°C; ◇, 530°C; △, 500°C; ○, 450°C [22].

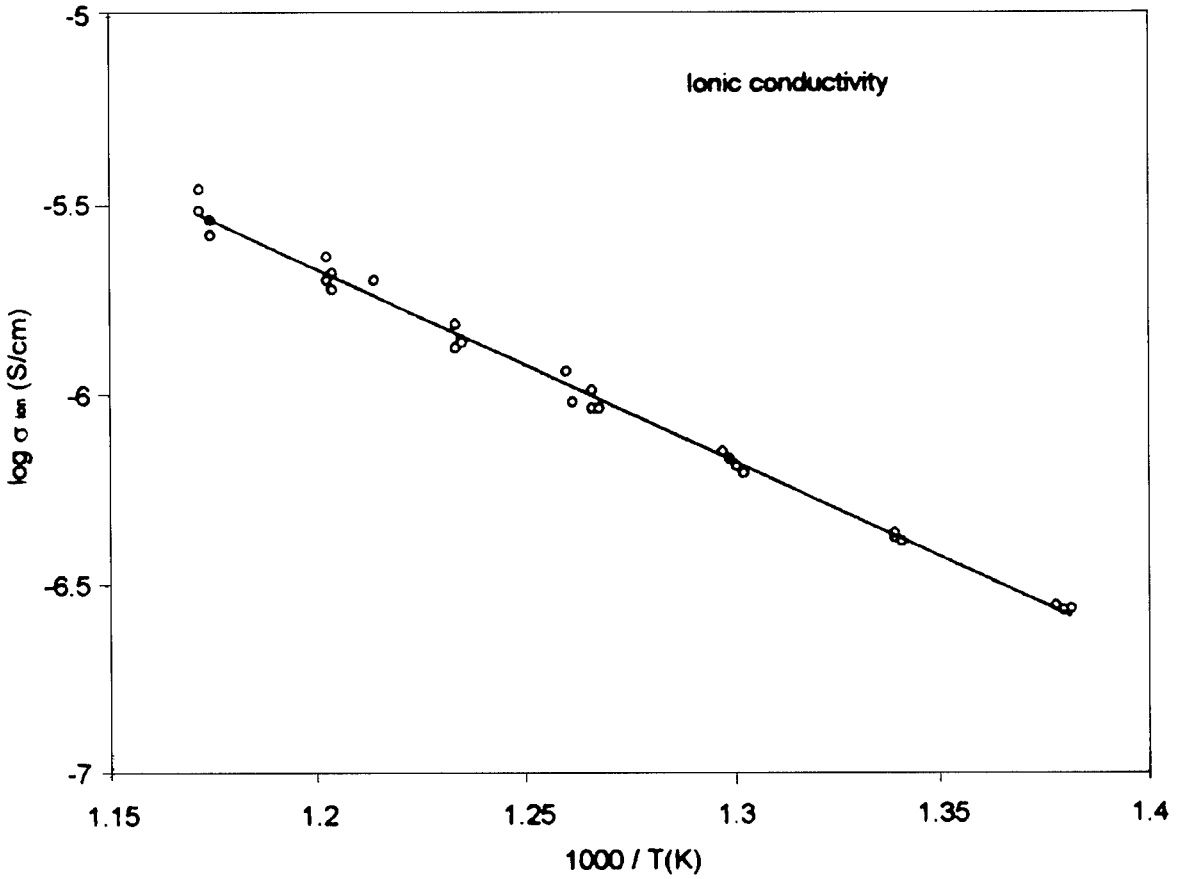

Fig. 13. The ionic conductivity of nanocrystalline TiO_2 as a function of reciprocal temperature [22].

line specimens with 50 and 260 nm grain size. They report activation energies of 0.96 and 1.23 eV respectively and considerably higher magnitudes of conductivity. It should be noted that the authors were able to stabilize the rutile phase by the addition of 1 mol% SnO_2 while the specimens of Knauth and Tuller [22] were prepared in the anatase phase. While one might wish to conclude that ionic conduction in the rutile phase is much higher than in the anatase phase, it must be remembered that the P_{O_2} independence of the conductivity suggests impurity control and at this point we have no clear means for comparing the effective dopant levels in the two sets of materials. On the contrary, the activation energies of the two sets of materials are similar (rutile 0.96 eV versus anatase 1.0 eV) for materials with similar grain size suggesting carrier rather than mobility control. Furthermore, more direct means for confirming the ionic nature of the conductivity in the P_{O_2} independent conductivity plateaus would be most desirable.

4. Conclusions

We have focused in this article on the question of whether and to what extent ionic conduction and/or defect formation are modified in nanocrystalline oxides. We have reviewed the literature on three systems; cubic zirconia, ceria and titania, for which

experimental data has become available. At this time, it is too early to make firm conclusions but we can make some useful observations. These include:

1. Additives which contribute to ion blocking at grain boundaries are diluted in nanocrystalline oxides giving rise to substantial reductions in specific grain boundary resistivities. This leads, in some cases, to an overall decrease in grain boundary resistance.
2. The case for enhanced ionic conduction in nominally undoped nanocrystalline oxides remains unresolved. In the case of CeO_2, enhanced electronic conductivity (see (4) below) masks any changes in ionic conductivity. In TiO_2, evidence is mixed. Nanocrystalline rutile appears to exhibit higher ionic conductivity than single crystal rutile while nanocrystalline anatase exhibits comparable levels of conductivity. In any case, more direct methods of measuring ionic conduction are necessary before even these tentative observations are taken too seriously.
3. There is mixed evidence in support of enhanced ionic conduction in doped electrolytes. No increases in ionic conduction are reported for either bulk stabilized ZrO_2 or doped CeO_2. In thin films, enhancements of several orders of magnitude are reported. It remains to be seen if this discrepancy is related to differences in the manner in which the dopants are distributed between grain and grain boundary during processing or, in the case of the films, are due to spurious effects such as humidity or film substrate interactions.
4. In CeO_2 or CeO_2-based solid solutions, there is strong support for the notion that the energetics for defect formation may be substantially reduced in nanocrystalline oxides. This results in markedly increased levels of nonstoichiometry and electronic carrier generation, likely important contributors to the enhanced catalytic activity reported for these materials. Similar observations, while less dramatic, have also been reported for TiO_2 [22].

One may confidently conclude that there remains much interesting work still to be done. Given recent improvements in the processing and characterization of nanocrystalline materials and structures, progress in this field can be expected to be rapid.

Acknowledgements

The author acknowledges close collaborations and/or discussions with P. Knauth, J. Maier, Y.M. Chiang, J. Ying, I. Kosacki and O. Porat. This work is being supported by the National Science Foundation under grants DMR 97-01699 (L. Schioler, program manager) and INT-98155788 as part of the US-France Cooperative Research Program. Thanks go to E. Anderson and H. Seh for manuscript preparation.

References

[1] H.L. Tuller, J. Electroceram. 4 (Suppl. 1) (1999) 33.
[2] S.P.S. Badwal, S. Rajendran, Solid State Ionics 70–71 (1994) 83.
[3] R. Gerhardt, A.S. Nowick, J. Am. Ceram. Soc. 69 (1986) 641.
[4] R. Gerhardt, A.S. Nowick, M.E. Mochel, I. Dumler, J. Am. Ceram. Soc. 69 (1986) 646.
[5] M. Aoki, Y.-M. Chiang, I. Kosacki, J.-R. Lee, H.L. Tuller, Y.J. Liu, J. Am. Ceram. Soc. 79 (1996) 1169.
[6] J. Maier, Prog. Solid State Chem. 23 (1995) 171.
[7] H.L. Tuller, P.K. Moon, Mat. Sci. Eng. B 1 (1988) 171.
[8] A. Atkinson, C. Monty, in: L.C. Dufour et al. (Ed.), Surfaces and Interfaces of Ceramic Materials, Kluwer Academic, Dordrecht, The Netherlands, 1989, p. 273.
[9] J.A. Cusumano, in: J.M. Thomas, K.I. Zmarev (Eds.), Perspectives in Catalysis, Blackwell Scientific, Boston, 1992.
[10] K.L. Merkle, Phys. Chem. Sol. 55 (1994) 991.
[11] Y.-M. Chiang, E.B. Lavik, I. Kosacki, H.L. Tuller, J.Y. Ying, J. Electroceramics 1 (1997) 7–14.
[12] J. Maier, Solid State Ionics 23 (1987) 59.
[13] H.L. Tuller, in: F.W. Poulsen, N. Bonanos, S. Linderoth, M. Mogensen, B. Zachau-Christiansen (Eds.), High Temperature Electrochemistry: Ceramics and Metals, Risø National Laboratory, Roskilde, 1996, p. 139.
[14] P. Mondal, H. Hahn, Ber. Bunsenges Phys. Chem. 101 (1997) 1765–1766.
[15] S. Jiang, J. Mat. Res. 12 (1997) 2374.
[16] I. Kosacki, B. Gorman, H.U. Anderson, in: T.A. Ramanarayanan, W.L. Worrell, H.L. Tuller, A.C. Kandkar, M. Mogensen, W. Gopel (Eds.), Ionic and Mixed Conductors, Vol. III, Electrochemical Society, Pennington, NJ, 1998, p. 631.
[17] H.L. Tuller, A.S. Nowick, J. Electrochem. Soc. 126 (1979) 209–217.

[18] H.L. Tuller, A.S. Nowick, J. Phys. Chem. Solids 38 (1977) 859–867.
[19] H.L. Tuller, Solid State Ionics 52 (1992) 135–146.
[20] A. Tschope, W. Liu, M. Flytzani-Stephanopolous, J.Y. Ying, J. Catal. 157 (1995) 42.
[21] A. Tschope, J.Y. Ying, H.L. Tuller, Sensors and Actuators B 31 (1996) 111.
[22] P. Knauth, H.L. Tuller, J. Appl. Phys. 85 (1999) 897–902.
[23] I. Kosacki, H. Anderson, Mat. Res. Proc. 453 (1997) 537.
[24] O. Porat, E.B. Lavik, H.L. Tuller, Y.-M. Chiang, in: S. Komarneni, J. Parker, H. Wollenberger (Eds.), Nanophase and Nanocomposite Materials, Vol. II, Materials Research Society, Pittsburgh, PA, 1997, p. 99.
[25] A. Tschöpe, R. Birringer, Nanostructured Mater. 9 (1997) 59.
[26] P. Knauth, H.L. Tuller, J. Euro. Ceram. Soc. 19 (1999) 831.
[27] E.B. Lavik, Y.M. Chiang, Mat. Res. Proc 457 (1997).
[28] Y.M. Chiang, E.B. Lavik, D.A. Blom, Nanostructured Mater. 9 (1997) 633.
[29] C.J. Barbe, F. Arendse, P. Compte et al., J. Am. Ceram. Soc. 80 (1997) 3157.
[30] J.Y. Ying, T. Sun, J. Electroceramics 1 (1997) 219.
[31] J. Nowotny, M. Redecka, M. Rekes, S. Sugihara, E.R. Vance, W. Weppner, Ceramics Int. 24 (1998) 571.
[32] C. Demetry, V. Shi, Solid State Ionics 118 (1999) 271.